Ionics (2020) 26:5233–5240
https://doi.org/10.1007/s11581-020-03598-2

ORIGINAL PAPER

$NiCo_2O_4$ functionalized with rGO catalyst as an active layer for ammonia sensing

G. Marimuthu[1] · G. Palanisamy[1] · T. Pazhanivel[1] · G. Bharathi[2] · K. P. Tiruppathi[3] · D. Nataraj[3]

Received: 26 November 2019 / Revised: 12 April 2020 / Accepted: 25 April 2020 / Published online: 8 June 2020

Abstract

Spinel $NiCo_2O_4$ material has received considerable attention as an excellent gas sensing material. In this study, we report facile and hydrothermal method synthesis for preparing mesoporous $NiCo_2O_4$ and its composite with reduced graphene oxide (rGO) by wet impregnation method. The as-prepared samples were subjected to structural and morphological investigations. The constructed $NiCo_2O_4$-rGO composite gas sensor shows superior NH_3 gas sensing performance at room temperature and the response for 100 ppm NH_3 is 1.068 at room temperature. Moreover, this sensor shows better gas sensing performances with fast response times, recovery times, and good repeatability for a test period of 10 cycles along with high selectivity for NH_3 gas sensor. Thus, $NiCo_2O_4$-rGO composite may be used as an efficient NH_3 gas sensor. The sensing mechanism of the $NiCo_2O_4$-rGO composite sensors has also been proposed in this paper.

Keywords $NiCo_2O_4$-rGO · Nanocomposite · Ammonia · Chemoresistive sensor

Introduction

Chemoresistive sensor based on metal oxides has been attracted for ammonia gas (NH_3) [1]. NH_3 can be indoor air pollutants which are widely used in various industries such as food industry, chemical plant, agriculture, chemical industry, and environmental monitoring [2–4]. The toxic gas (NH_3) exposure can cause irritation to the skin, eyes, nose, mouth, and lungs [2, 5]. The acute exposure to high concentrations of ammonia causes headache, vomiting, dyspnea, pneumonedema, and even death. According to the occupational safety and health administration (OSHA) directed, the ammonia in the work place is limited to 50 ppm [6] .Consequently, the essential need of reliable and real ammonia gas sensor is urgent [1]. Therefore, it was very important to develop an ammonia sensor with fast response time, high selectivity, low power, and low detection limit, cost at room temperature for practical applications.

Due to its multifunctional characteristics, spinel-type materials, having a general formula of AB_2O_4, have shown great promise in supercapacitor applications [7], gas sensing [8], and lithium-ion batteries [9]. Recently, the spinel-structured materials have been used for the design of gas sensing material with improved sensing response and selectivity. $CuCo_2O_4$ [10], $ZnCo_2O_4$ [11], and $MgCo_2O_4$ [12] are some of the most widely investigated gas sensors for the detection of toxic gases. One such interesting spinel type is $NiCo_2O_4$, which offers more active sites suitable for several suitable applications. However, for the low sensitivity and poor response and recovery of individual $NiCo_2O_4$, nanostructure poses a serious challenge in using them for gas sensing applications [13]. Until date, some conductive materials have been used to improve the gas sensing properties of the $NiCo_2O_4$ nanostructured materials. Wu J et al. used rGO as a composite material with $NiCo_2O_4$ to get the improved gas sensing performances. In this perspective, graphene-based materials would be a better choice as composite, which would enhance the gas sensing properties of $NiCo_2O_4$, without affecting its primary properties [14].

✉ T. Pazhanivel
pazhanit@gmail.com

[1] Smart Materials Interface Laboratory, Department of Physics, Periyar University, Salem, Tamil Nadu 636 011, India

[2] Key Laboratory of Optoelectronic Devices and Systems of Guangdong Province, College of Optoelectronic Engineering, Shenzhen University, Shenzhen, Guangdong Province 518060, People's Republic of China

[3] Low Dimensional Materials Laboratory, Department of Physics, Bharathiar University, Coimbatore, Tamil Nadu 641 046, India

Graphene, a unique two-dimensional material (2D), has attracted considerable attention of technologists in a variety of applications especially in the charge transport area, because of its excellent electronic conducting properties [15] with extremely high electron mobility [16]. Pristine graphene has several complications in preparing and the reduced graphene oxide (rGO) is its nearest analogue, which can be prepared by solution processing techniques. Recent investigations revealed that the use of reduced graphene oxide with mixed metal oxide nanoparticles can improve the gas sensing performance in terms of high sensitivity at room temperature [17].

In the present study, we have prepared the $NiCo_2O_4$ and $NiCo_2O_4$-rGO nanocomposite for the detection of NH_3. After careful investigation of structural and morphological properties, the $NiCo_2O_4$ and $NiCo_2O_4$-rGO nanocomposite formations were confirmed. The as-prepared samples were than used to construct the gas sensors and tested against three different gases. The constructed sensors show high selectivity against NH_3 gas. The $NiCo_2O_4$-rGO nanocomposite sensor shows better sensing performances along with fast response and recovery times. The stability of the constructed sensor is also studied and the obtained results were discussed in detail.

Chemicals

All the reagents were purchased commercially and used as without further purification. Nickel chloride hexahydrate ($NiCl_2{\cdot}6H_2O$), cobalt chloride hexahydrate ($CoCl_2{\cdot}6H_2O$), graphite powder, hydrogen peroxide, sulfuric acid, potassium permanganate, sodium nitrate, hydrochloric acid, cetyl trimethyl ammonium bromide (CTAB), and urea were purchased from Merck, India. All experiments were performed using deionized (DI) water with an electrical conductivity > 18 MΩ (S/m).

Preparation of reduced graphite oxide nanosheet

Graphene oxide (GO) was prepared by modified Hummer's method and it is reduced by the following procedure to get reduced graphene oxide (rGO) [16]. One gram of as-synthesized GO powder was dispersed in 50-ml DI water using bath sonicator for 2 h and then 20 ml of ammonia solution was drop wise added into the solution. Then the solution was transferred in a 100-ml Teflon-lined autoclave and heated at 160 °C for 12 h in hot air oven. After that, the autoclave was allowed to cool naturally in the room temperature. The black precipitate was collected and washed with ethanol and DI water several times. Finally, the collected sample was dried in a hot air oven at 60 °C overnight [18].

Preparation of $NiCo_2O_4$ nanorod

Hydrothermal synthesis of nanorod $NiCo_2O_4$ samples was reported in our previous work [18]. In a typical synthesis, 30 (mmol) $NiCl_2{\cdot}6H_2O$ and 60 (mmol) $CoCl_2{\cdot}6H_2O$ (Ni and Co, molar ratio 1:2) were dissolved in 100 ml of deionized water and added 30 (mmol) CTAB dissolved in 100 ml of water. The mixture was stirred for 1 h to form homogeneous solution. Ninety (mmol) of solid urea was added to this solution and stirring was continued for three more hours to achieve complete homogeneity. The resulting solution was transferred into Teflon-lined stainless steel autoclaves of 200-ml capacity. The reactions in these autoclaves were carried out at120 °C, in an electrical oven for 48 h. The autoclaves were cooled to room temperature and the light pink–colored precipitates were separated by centrifuging at 4000 rpm. The product was repeatedly washed with deionized water, mixture of water and absolute ethanol, and finally with absolute ethanol for three times. The obtained products were dried in an oven at 60 °C for 12 h and calcined at 350 °C for 3 h.

Preparation of $NiCo_2O_4$-rGO composite

$NiCo_2O_4$-rGO composite was prepared by wet impregnation method [19]. 2:1 weight ratios of $NiCo_2O_4$ nanorod were added separately with rGO nanosheets in to 15 ml of ethanol. The resulting solution was continuously stirred and subsequently heated at 60 °C to evaporate the solvent. Then, the obtained $NiCo_2O_4$-rGO composite was dried for 6 h, collected, and stored for further processes.

Characterization techniques

The phase purity and crystal structure of the as-prepared samples were characterized by powder X-ray diffraction (XRD) using Rigaku D/Max Ultima III X-ray diffractometer with a Cu Kα radiation source (0.154 nm) operated at 40 kV. Fourier-transform infrared (FT-IR) spectra of KBr powder–pressed pellets were recorded by Bruker a NEXUS 470 in the range of 4000 to 400 cm^{-1}. The surface morphology of obtained samples was visualized by field emission scanning electron microscopy (FESEM, Hitachi S-4800) and high-resolution transmission electron microscopy (HRTEM, JEM-2100). Nitrogen adsorption-desorption isotherm measurements were performed on AUTOSORB-1-MP to study the specific surface area.

Preparation and gas sensor fabrication

A 0.5 g of the $NiCo_2O_4$-rGO nanopowder was grounded well in an agate mortar for 10 min and then samples were mixed with 0.5 ml of the deionized water and subsequently, grounded for another 10 min to obtain a black slurry with good stability. The ceramic tube (diameter 1 mm and length 4.0 mm) was furnished with gold signal electrodes and homogeneous black paste with the sensor element was coated on a ceramic tube. Further heating was done to remove excess water molecules and improve contact between $NiCo_2O_4$-rGO with gold electrode. The sensor device was placed in a chamber. A constant voltage of + 2 V was applied to the sensor device. The gas sensing measurements were carried out using Keysight source meter. The source meter was coupled to the computer via the RS 232 interface to record the change in resistance with respect to time. The sensing measurement cycle is as follows: nitrogen (N_2) 150 sccm was introduced as the carrier gas, The change in resistance *R* and the resistance of the sensor was calculated [20].

$$S = \mathrm{Rg}/\mathrm{Ra}$$

where Rg and Ra were the resistance of the sensor in NH_3 and air atmospheres, respectively

Results and discussion

The XRD patterns of rGO, $NiCo_2O_4$, and $NiCo_2O_4$-rGO nanocomposite are shown in Fig. 1. The successful reduction of GO into rGO is confirmed by the peak observed around 25.58°, which is attributed to the (022) plane [21]. The $NiCo_2O_4$ and $NiCo_2O_4$-rGO composite samples produced several diffraction peaks around 19.20°, 31.36°, 36.96°, 38.63°,44.91°, 55.71°, 65.29°, and 77.42°, which are indexed to (111), (220), (311), (222), (400), (422), (511), and (440) crystal plans, matching with the standard values (JCPDS no. 73-1702). Absence of additional peaks reveals that there were no impurities or other crystal phases present in the sample. The similarity in the diffraction peaks of $NiCo_2O_4$ and $NiCo_2O_4$-rGO composite samples indicate that the incorporation of rGO with $NiCo_2O_4$ did not affect the crystal structure properties of $NiCo_2O_4$. Also the absence of rGO diffraction peak in the $NiCo_2O_4$- rGO composite sample is attributed to the less amount of rGO when compared with the $NiCo_2O_4$. The crystallite size values calculated using the Debye Scherer formula [16] are 43 and 40 nm for $NiCo_2O_4$ and $NiCo_2O_4$-rGO samples, respectively. The variation in the crystalline size after addition of rGO is an indication of $NiCo_2O_4$-rGO composite formation. In order to investigate further the rGO, $NiCo_2O_4$ and $NiCo_2O_4$-rGO composite samples were subjected to FT-IR spectroscopy analysis.

Figure 2 shows FT-IR spectra of rGO, $NiCo_2O_4$, and $NiCo_2O_4$-rGO composite samples. The FT-IR spectrum of rGO sample displays two peaks in the range of 3500–4000 cm^{-1} corresponding hydroxyl and amine groups. The amine group could possibly be included from the ammonia, which is added for the reduction of GO into rGO in the hydrothermal reduction process. The peaks at 1196 and 1562 cm^{-1} are attributed to C–OH and C=O groups, respectively, thereby confirming the formation of functional groups rGO [22, 23]. The formation of $NiCo_2O_4$ is indicated by two strong peaks around 561 and 654 cm^{-1}, which can be assigned to the stretching vibration of the Ni–O and Co–O bond, and is reported elsewhere [15]. The $NiCo_2O_4$-rGO composite sample contains the FT-IR fingerprints corresponding to both the $NiCo_2O_4$ with rGO, which further confirms the composite formation.

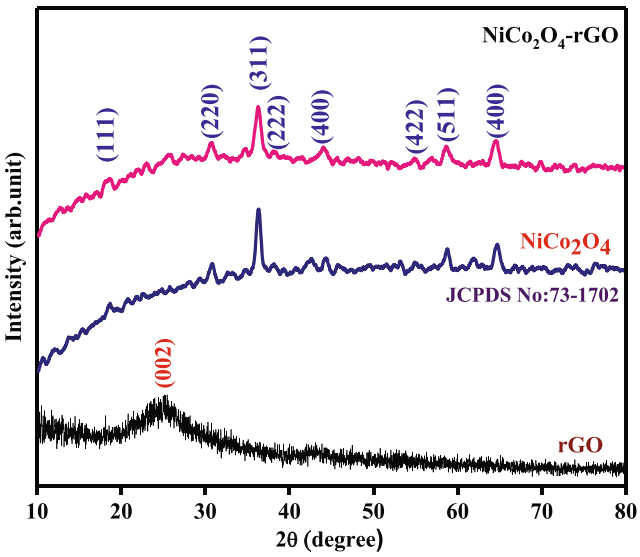

Fig. 1 Typical XRD patterns of all samples

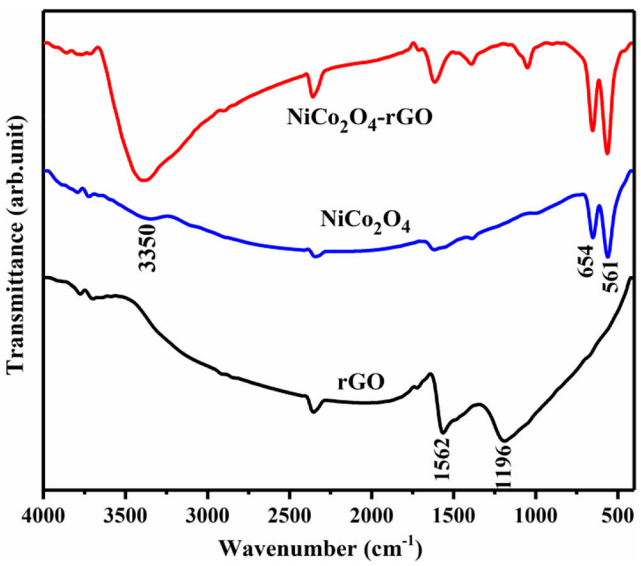

Fig. 2 FT-IR spectra of rGO, $NiCo_2O_4$, and $NiCo_2O_4$-rGO

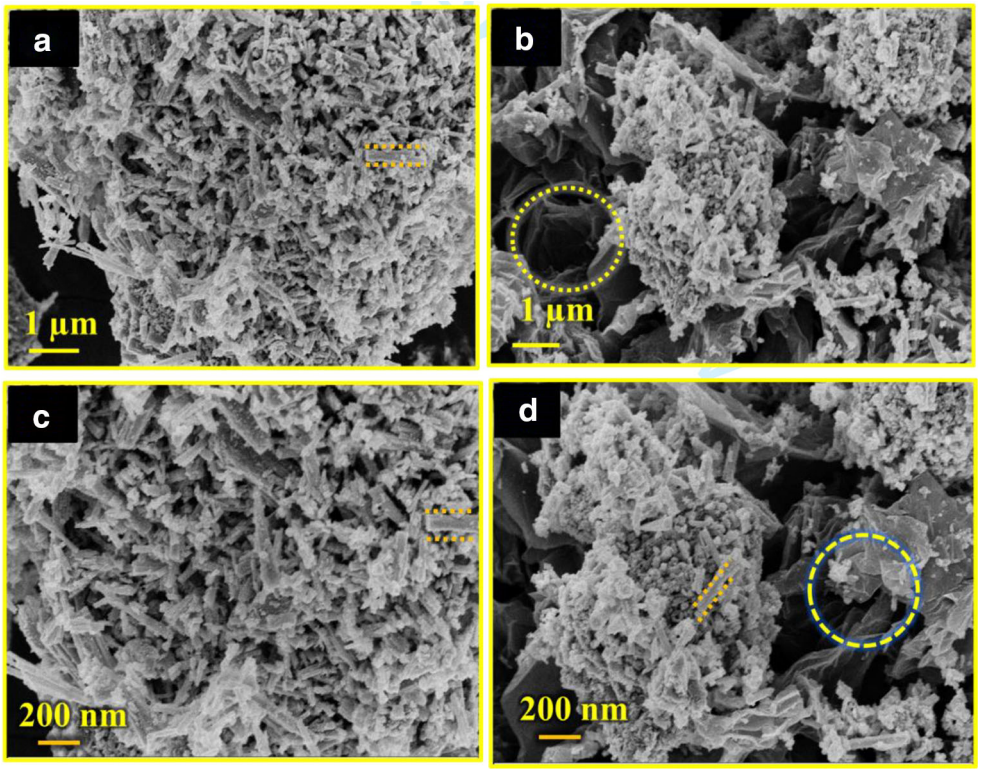

Fig. 3 Low and high-resolution FESEM images of $NiCo_2O_4$ (**a**, **c**) and $NiCo_2O_4$-rGO (**b**, **d**) samples

The as-prepared $NiCo_2O_4$ and $NiCo_2O_4$-rGO composite samples were then subjected to FESEM analysis in order to investigate the morphology. As presented in Fig. 3(a), (d), both the samples display aggregated nanorod structure. The observed morphology is highly porous, because the aggregation took place in particular centers. In others words, the nanorods are not aggregated one over the other, instead, they are attached to a particular center and formed a bunch-like structure. It is because of this interesting morphology, the samples are highly porous in nature, which would benefit the adsorption and desorption of gas. In addition, the change in morphology is observed in the case of $NiCo_2O_4$-rGO composite, in which the big bunch-like aggregated nanorod structure was split into smaller aggregations. This change in morphology is attributed to the incorporation of $NiCo_2O_4$ with rGO [13].

After that, the detailed morphology of the as-prepared nanocomposite was investigated through high-resolution transmission electron microscopy (HRTEM) as represented in Fig. 4(a). The $NiCo_2O_4$ bunch-like nanorod can be seen uniformly distributed on rGO nanosheet. It further revealed the typical bunch-like nanorod structural characteristic of $NiCo_2O_4$ anchored on graphene oxide sheets in the composites. Figure 4(b) shows the HRTEM image of an individual $NiCo_2O_4$ nanorod with a lattice spacing of 0.23 nm well-matched the (311) lattice planes of cubic spinel $NiCo_2O_4$, respectively. These results further confirmed the existence of

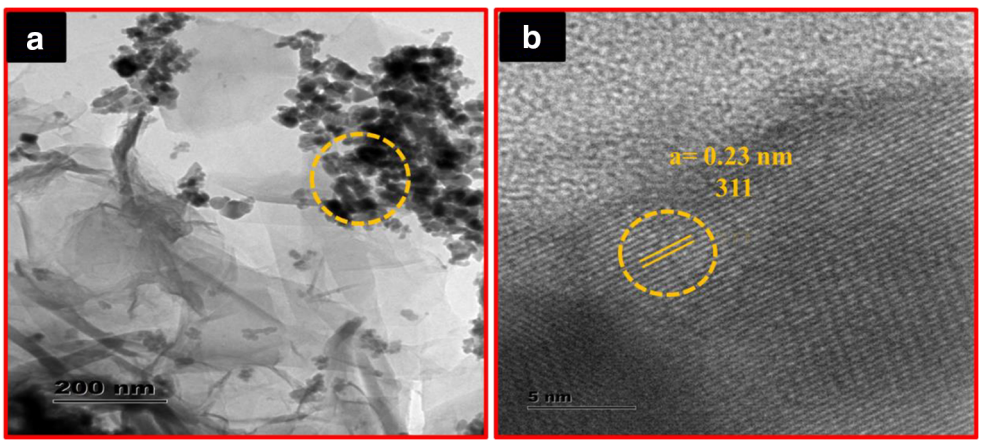

Fig. 4 (**a**, **b**) HRTEM image of $NiCo_2O_4$-rGO nanorod

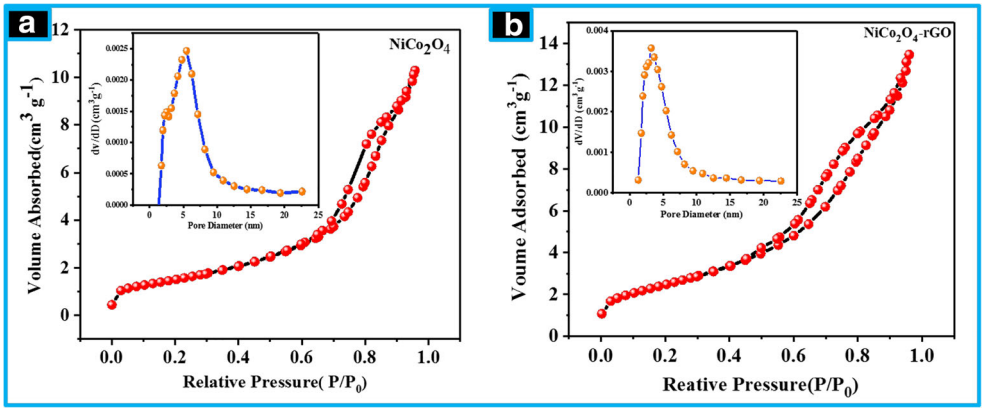

Fig. 5 (**a**, **b**) N_2 adsorption-desorption isotherms of the $NiCo_2O_4$ and $NiCo_2O_4$-rGO nanocomposite

$NiCo_2O_4$, which was in agreement with the above-revealed XRD results.

This porous morphology is further investigated by nitrogen adsorption and desorption kinetics, in order to understand its role in the gas sensing performances. The specific surface area and the pore size distribution are the vital factors in understanding the gas sensing performances of the as-prepared sample. The nitrogen adsorption-desorption isotherms of $NiCo_2O_4$ and $NiCo_2O_4$-rGO composite samples were measured at 77 k using N_2 adsorbent and presented in Fig. 5(a), (b) [17]. The BET isotherms of $NiCo_2O_4$ and $NiCo_2O_4$-rGO sample exhibit type IV characteristics, which indicate that the sample contains a certain amount of mesoporous structure. The calculated BET-specific surface area for $NiCo_2O_4$ and $NiCo_2O_4$-rGO samples are 5 and 9 m^2g^{-1}, and their corresponding pore volumes are 0.957 and 0.960 $cm^3\ g^{-1}$, respectively [24].

Gas sensing performance

The gas sensing performances of $NiCo_2O_4$ and $NiCo_2O_4$-rGO composite samples were evaluated against NH_3 gas. Figure 6(a) shows the comparison of sensing response (S) between $NiCo_2O_4$ and $NiCo_2O_4$-rGO nanocomposite with 100 ppm NH_3 at room temperature. It is notable that the response (1.068) of $NiCo_2O_4$-rGO nanocomposite to 100 ppm NH_3 gas is greater than that of pure $NiCo_2O_4$ sensing response

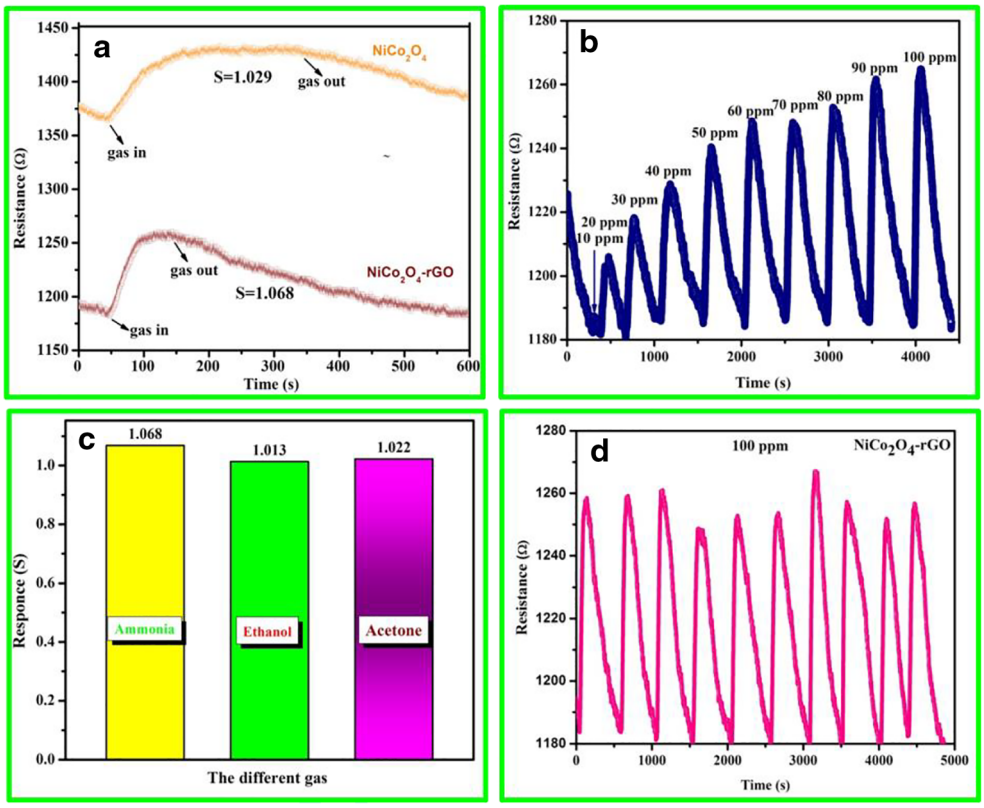

Fig. 6 (**a**) Comparison of response-recovery time curve of $NiCo_2O_4$-rGO and $NiCo_2O_4$ to 100 ppm NH_3 gas. (**b**) Gas sensing response of the $NiCo_2O_4$-rGO to different concentration of NH_3. (**c**) The same sensor with several other gases to NH_3. (**d**) Stability of the $NiCo_2O_4$-rGO sensor to NH_3

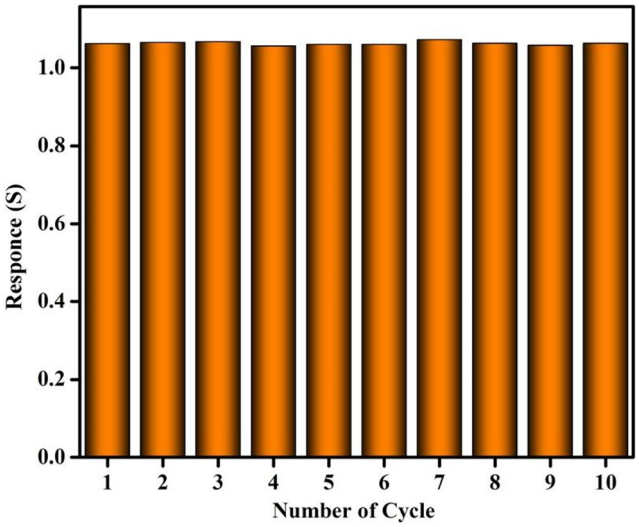

Fig. 7 Response cycle stability of the $NiCo_2O_4$-rGO sensor to NH_3

(1.029). The active sensing responses of $NiCo_2O_4$-rGO nanocomposite–based gas sensors by varying the NH_3 concentration 10 to 100 ppm at room temperature are shown in Fig. 6(b). It is clear that the $NiCo_2O_4$-rGO composite sensor exhibits better response intensity with increasing gas concentrations and the sensor can completely recover to its initial state. Figure 6(c) shows the selectivity of the $NiCo_2O_4$-rGO nanocomposite investigated against by various toxic gases such as ammonia (NH_3), ethanol (C_2H_6O), and acetone (C_3H_6O). In comparison, it is clear that the constructed $NiCo_2O_4$-rGO composite–based gas sensor is highly selective against NH_3 gas and it is attributed to the lower molecular size (0.32 nm) and low dipole moment (1.4 nm) of the NH_3, when compared with the other two gases (the molecular size and dipole moment of ethanol (C_2H_6O) and acetone (C_3H_6O) are 0.44 nm and 0.66 nm, and 1.69 nm and 2.88 nm, respectively) the stability of the $NiCo_2O_4$-rGO composite–based gas sensor is investigated by admitting 100 ppm NH_3 gas over 10 cycles. In sensor, the stability and repeatability are important

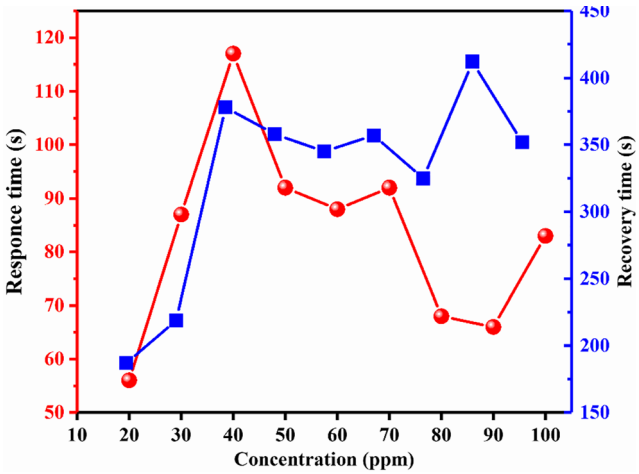

Fig. 8 Response-recovery time curve of $NiCo_2O_4$-rGO

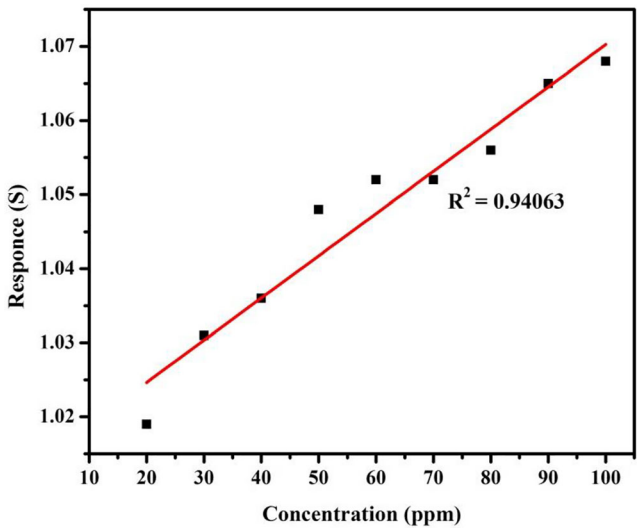

Fig. 9 Linear dependence of response of $NiCo_2O_4$-rGO sensor on different concentration of NH_3 at room temperature

parameters for gas sensor optimizations. In Figs. 6(d) and 7, a slight variation in higher resistance point, for each cycle, may be due to the poor adhesion between sensing layer and subtract [25]. Figure 8 shows the response-recovery times of $NiCo_2O_4$-rGO samples (10 to 100 ppm) NH_3. The $NiCo_2O_4$-rGO sample exhibits fast response (57 s) time and recovery (185 s) time at 20 ppm as compared with other contraction. This improved performance is attributed to the heterojunction formed between $NiCo_2O_4$ and rGO, in which the rGO acted as 1D conductive network for the electron transfer process.

Figure 9 shows the sensor response versus different NH_3 gas concentration in the range of 10–100 ppm. The correlation coefficient R^2 of the fitting curve in the range is to be 0.9496, indicating good linearity in the sensing measurement. This linear behavior is suitable for approximation of NH_3 in practical sensing application. Furthermore, from the above observation, it can be concluded that the availability of active sites for adsorption on the sensor material decreased with the increase in NH_3 concentration [26].

Gas sensing mechanism

Semiconductor metal oxide–based sensors work on the principle of the change in resistance corresponding to the reaction between gas molecules and the sensitive surface. This involves gas adsorption, surface reaction, and desorption processes [20]. Initially, when the $NiCo_2O_4$ surface is exposed to air atmosphere, the air molecules are adsorbed into the $NiCo_2O_4$ surface and capture electrons from the $NiCo_2O_4$ surface. This results in the formation of a hole accumulation layer (HAL) on the surface of $NiCo_2O_4$, which eventually results in the decrease of resistance. Upon exposure to the NH_3 (strong reducing agents), the pre-adsorbed oxygen ion

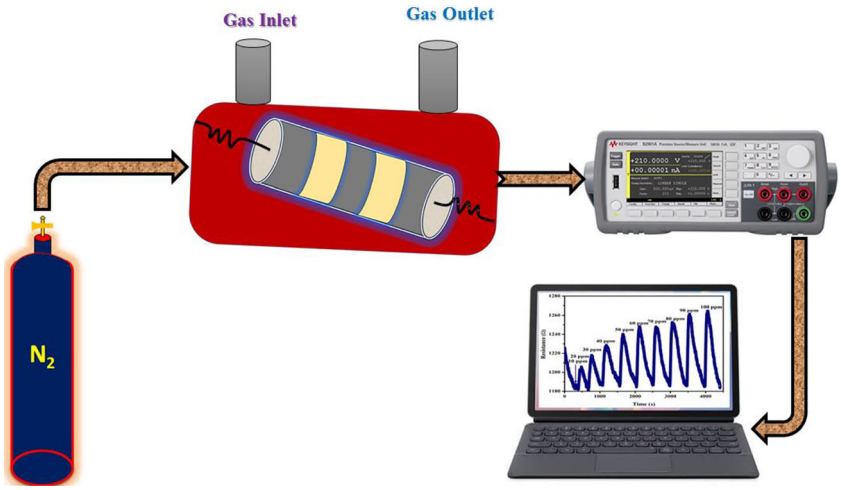

Fig. 10 Schematic diagram of the gas-sensing test

on the $NiCo_2O_4$ surface reacts with NH_3 and the resistance of the sensing element increases, which obeys the p-type behavior of $NiCo_2O_4$.The sensing performance of $NiCo_2O_4$-rGO nanocomposites can also be explained using schematic diagram shown Fig. 10,except the fast response and recovery. It is caused by the hybridizing rGO, which triggers the fast electron transfer between the sensing element and the electrode [27]. From the above observations, it is clear that the room temperature NH_3 sensing performance of $NiCo_2O_4$-rGO composite gas sensor can be attributed to two key factors: (i) the mesoporous structure of $NiCo_2O_4$-rGO nanocomposite which provided surface accessibility for the interaction with the analyte gas, and (ii) the fast charge transfer initiated by the rGO, which resulted in better response and recovery times.

Conclusions

In conclusion, a cost-effective $NiCo_2O_4$-rGO nanocomposite–based gas sensor was developed and its room temperature NH_3 gas sensing properties were demonstrated. Before the construction of gas sensor, the nanocomposite sample was characterized by several analytical techniques such as XRD, FT-IR, FESEM, HRTEM, and BET analysis. The better performance of $NiCo_2O_4$-rGO nanocomposite–based gas sensor is due to its mesoporous structure and fast charge transfer initiated by the rGO. With high selectivity, sensitivity, and stability, our sensor can be used in practical applications.

References

1. Zito CA, Perfecto TM, Fonseca CS, Volanti DP (2018) Effective reduced graphene oxide sheets/hierarchical flower-like NiO composites for methanol sensing under high humidity. New J Chem 42: 8638–8645. https://doi.org/10.1039/c8nj01061g
2. Tabrizi L, Chiniforoshan H (2017) High-performance room temperature gas sensor based on gold(III) pincer complex with high sensitivity for NH3. Sensors Actuators B Chem 245:815–820. https://doi.org/10.1016/j.snb.2017.01.193
3. Wu DQ, Wu LL, Cui HC, Zhang HN, Yu JY (2016) A rapid ammonia sensor based on lysine nanogel-sensitized PANI/PAN nanofibers. J Mater Chem B 4:1520–1527. https://doi.org/10.1039/c5tb02058a
4. Qin Z, Zeng D, Zhang J, Wu C, Wen Y, Shan B, Xie C (2017) Effect of layer number on recovery rate of WS_2 nanosheets for ammonia detection at room temperature. Appl Surf Sci 414:244–250. https://doi.org/10.1016/j.apsusc.2017.04.063
5. Yoo KP, Kwon KH, Min NK, Lee MJ, Lee CJ (2009) Effects of O_2 plasma treatment on NH_3 sensing characteristics of multiwall carbon nanotube/polyaniline composite films. Sensors Actuators B Chem 143:333–340. https://doi.org/10.1016/j.snb.2009.09.029
6. Poloju M, Jayababu N, Ramana Reddy MV (2018) Improved gas sensing performance of Al doped ZnO/CuO nanocomposite based ammonia gas sensor. Mater Sci Eng B 227:61–67. https://doi.org/10.1016/j.mseb.2017.10.012
7. Hao C, Zhou S, Wang J, Wang X, Gao H, Ge C (2018) Preparation of hierarchical spinel $NiCo_2O_4$ nanowires for high-performance supercapacitors. Ind Eng Chem Res 57:2517–2525. https://doi.org/10.1021/acs.iecr.7b04412
8. Vadivel S, Balaji G, Rathinavel S (2018) High performance ethanol and acetone gas sensor based nanocrystalline $MnCo_2O_4$ using clad-modified fiber optic gas sensor. Opt Mater 85:267–274. https://doi.org/10.1016/j.optmat.2018.08.067
9. Natarajan S, Anantharaj S, Tayade RJ, et al (2017) Recovered spinel $MnCo_2O_4$ from spent lithium-ion batteries for enhanced electrocatalytic oxygen evolution in alkaline medium
10. Jain S, Patrike A, Badadhe SS, Bhardwaj M, Ogale S (2018) Room-temperature ammonia gas sensing using mixed-valent $CuCo_2O_4$ nanoplatelets: performance enhancement through stoichiometry control. ACS Omega 3:1977–1982. https://doi.org/10.1021/acsomega.7b01958
11. Long H, Harley-Trochimczyk A, Cheng S, Hu H, Chi WS, Rao A, Carraro C, Shi T, Tang Z, Maboudian R (2016) Nanowire-assembled hierarchical $ZnCo_2O_4$ microstructure integrated with a low-power microheater for highly sensitive formaldehyde detection. ACS Appl Mater Interfaces 8:31764–31771. https://doi.org/10.1021/acsami.6b11054
12. Rathinavel S, Vadivel S, Balaji G (2019) Development of ethanol and acetone gas sensing performance of $MgCo_2O_4$ nanosensors by clad modified fiber optical method. Opt Fiber Technol 48:218–224. https://doi.org/10.1016/j.yofte.2019.01.016

13. Rao H, Zhang Z, Ge H, Liu X, Zou P, Wang X, Wang Y (2017) Enhanced amperometric sensing using a $NiCo_2O_4$/nitrogen-doped reduced graphene oxide/ionic liquid ternary composite for enzyme-free detection of glucose. New J Chem 41:3667–3676. https://doi.org/10.1039/c7nj00077d
14. Wu J, Yang Y, Yu H, Dong X, Wang T (2019) Ultra-efficient room-temperature H 2 S gas sensor based on $NiCo_2O_4$ /r-GO nanocomposites. New J Chem 43:10501–10508. https://doi.org/10.1039/C9NJ01094G
15. Umeshbabu E, Rajeshkhanna G, Justin P, Rao GR (2016) $NiCo_2O_4$/rGO hybrid nanostructures for efficient electrocatalytic oxygen evolution. J Solid State Electrochem 20:2725–2736. https://doi.org/10.1007/s10008-016-3278-4
16. Du F, Zuo X, Yang Q et al (2016) The stabilization of $NiCo_2O_4$ nanobelts used for catalyzing triiodides in dye-sensitized solar cells by the presence of RGO sheets. Sol Energy Mater Sol Cells 149:9–14. https://doi.org/10.1016/j.solmat.2015.11.025
17. Bai S, Du L, Sun J et al (2016) Preparation of reduced graphene oxide/Co_3O_4 composites and sensing performance to toluene at low temperature. RSC Adv 6:60109–60119. https://doi.org/10.1039/c6ra06542b
18. Umeshbabu E, Rajeshkhanna G, Justin P, Rao GR (2015) Magnetic, optical and electrocatalytic properties of urchin and sheaf-like $NiCo_2O_4$ nanostructures. Mater Chem Phys 165:235–244. https://doi.org/10.1016/j.matchemphys.2015.09.023
19. Bai S, Liu H, Sun J, Tian Y, Luo R, Li D, Chen A (2015) Mechanism of enhancing the formaldehyde sensing properties of Co_3O_4 via Ag modification. RSC Adv 5:48619–48625. https://doi.org/10.1039/c5ra05772h
20. Tong X, Shen W, Chen X, Corriou J (2017) A fast response and recovery H_2S gas sensor based on free-standing TiO_2 nanotube array films prepared by one-step anodization method. Ceram Int 0–1. https://doi.org/10.1016/j.ceramint.2017.07.165
21. Zhang D, Liu J, Chang H, Liu A, Xia B (2015) Characterization of a hybrid composite of SnO_2 nanocrystal-decorated reduced graphene oxide for ppm-level ethanol gas sensing application. RSC Adv 5:18666–18672. https://doi.org/10.1039/c4ra14611e
22. Gong Y, Li D, Fu Q, Pan C (2015) Influence of graphene microstructures on electrochemical performance for supercapacitors. Prog Nat Sci Mater Int 25:379–385. https://doi.org/10.1016/j.pnsc.2015.10.004
23. Light V (2017) Photochemical oxidative coupling of 2-naphthols using hybrid rGO / MnO_2. https://doi.org/10.1002/cctc.201701470
24. Fan C, Ying Z, Zhang W, Ju T, Li B (2018) $NiCo_2O_4$ grown on Co/C hybrid nanofiber film with excellent electrochemical performance for flexible supercapacitor electrodes. J Mater Sci Mater Electron 29:6909–6915. https://doi.org/10.1007/s10854-018-8677-0
25. Hung CM, Hoa ND, Van Duy N et al (2016) Synthesis and gas-sensing characteristics of α-Fe_2O_3 hollow balls. J Sci Adv Mater Devices 1:45–50. https://doi.org/10.1016/j.jsamd.2016.03.003
26. Mounasamy V, Mani GK, Ponnusamy D, Tsuchiya K, Prasad AK, Madanagurusamy S (2018) Template-free synthesis of vanadium sesquioxide (V_2O_3) nanosheets and their room-temperature sensing performance. J Mater Chem A 6:6402–6413. https://doi.org/10.1039/c7ta10159g
27. Basyooni MA, Zaki SE, Ertugrul S, Yilmaz M, Eker YR (2020) Response of CO_2 room temperature gas sensor based on mixed-valence phases in molybdenum and tungsten oxide nanostructured thin films. Ceram Int 46:9839–9853. https://doi.org/10.1016/j.ceramint.2019.12.259